Two possible source regions for Central Greenland last glacial dust

Gábor Újvári[1,2], Thomas Stevens[3], Anders Svensson[4], Urs S. Klötzli[5], Christina Manning[6], Tibor Németh[1], János Kovács[7,8], Mark R. Sweeney[9], Martina Gocke[10], Guido L.B. Wiesenberg[10], Slobodan B. Markovic[11], Michael Zech[12]

[1]Institute for Geological and Geochemical Research, Research Centre for Astronomy and Earth Sciences, Hungarian Academy of Sciences, H-1112 Budapest, Budaörsi u. 45., Hungary

[2]Geodetic and Geophysical Institute, Research Centre for Astronomy and Earth Sciences, Hungarian Academy of Sciences, H-9400 Sopron, Csatkai E. u. 6-8., Hungary

[3]Department of Earth Sciences, Uppsala University, Villavägen 16, 75236 Uppsala, Sweden

[4]Centre for Ice and Climate, Niels Bohr Institute, University of Copenhagen, Juliane Maries Vej 30, 2100 Copenhagen, Denmark

[5]Department of Lithospheric Research, University of Vienna, Althanstraße 14, 1090 Vienna, Austria

[6]Department of Earth Sciences, Royal Holloway University of London, Egham, London, TW20 0EX, UK

[7]Department of Geology and Meteorology, University of Pécs, H-7624 Pécs, Ifjúság u. 6., Hungary

[8]Environmental Analytical and Geoanalytical Research Group, Szentágothai Research Centre, H-7624 Pécs, Ifjúság u. 20., Hungary

[9]Department of Earth Sciences, University of South Dakota, 414 E. Clark Street, Vermillion, SD 57069, USA

[10]Department of Geography, University of Zürich, Winterthurerstrasse 190, CH-8057 Zürich, Switzerland

[11]Laboratory for Palaeoenvironmental Reconstruction, Faculty of Sciences, University of Novi Sad, Trg Dositeja Obradovića 2, 21000 Novi Sad, Serbia

[12]Department of Soil Physics and Chair of Geomorphology, University of Bayreuth, Universitätsstrasse 30, D-95440 Bayreuth, Germany

Corresponding author: G. Újvári, Research Centre for Astronomy and Earth Sciences, Hungarian Academy of Sciences, H-9400 Sopron, Csatkai E. u. 6-8., Hungary. Email: ujvari.gabor@csfk.mta.hu

Key points

- New clay mineral and Sr–Nd–Hf data for last glacial Greenland dust sources
- Clay and Sr–Nd data suggest two equally plausible Greenland dust sources
- Hf isotopes of fine grain loess separates may be source-diagnostic

Abstract

Dust in Greenland ice cores is used to reconstruct the activity of dust emitting regions and atmospheric circulation. However, the source of dust material to Greenland over the last glacial period is the subject of considerable uncertainty. Here we use new clay mineral and <10 μm Sr–Nd isotopic data from a range of Northern Hemisphere loess deposits in possible source regions alongside existing isotopic data to show that these methods cannot discriminate between two competing hypothetical origins for Greenland dust: an East Asian and/or Central European source. By contrast, Hf isotopes (<10 μm fraction) of loess samples show considerable differences between the potential source regions. We attribute this to a first-order clay mineralogy dependence of Hf isotopic signatures in the finest silt/clay

fractions, due to absence of zircons. As zircons would also be absent in Greenland dust, this provides a new way to discriminate between hypotheses for Greenland dust sources.

Keywords: Greenland dust; origin; clay mineralogy; Sr-Nd-Hf isotopes; provenance

1. Introduction

Wind-borne mineral aerosol (here referred to as 'dust') influences global climate directly and indirectly through diverse physical and biogeochemical processes and is therefore considered a major component of the climate system [*Harrison et al.*, 2001; *Tegen*, 2003]. Dust particles affect the radiation budget through scattering and absorption of incoming solar and outgoing infrared radiation [*Tegen and Lacis*, 1996; *Liao and Seinfeld*, 1998], and by altering cloud optical properties, amounts and lifetimes [*Albrecht*, 1989; *Yin et al.*, 2002; *Andreae and Rosenfeld*, 2008]. Furthermore, airborne mineral dust provides micronutrients (e.g. iron, silica) to marine and terrestrial ecosystems [*Martin*, 1990; *Duce and Tindale*, 1991; *Falkowski et al.*, 1998], thereby affecting productivity, influencing the carbon cycle, and eventually atmospheric greenhouse gas content [*Archer et al.*, 1998; *Mahowald et al.*, 2005].

Dust not only affects climate, but the generation and transport of dust itself is extremely sensitive to climate and environmental change. As recorded in ice cores [*Thompson and Mosley-Thompson*, 1981; *Steffensen*, 1997; *Lambert et al.*, 2008], marine [e.g. *Winckler et al.,* 2008] and terrestrial sediments [e.g. loess; *Kohfeld and Harrison*, 2001; *Derbyshire*, 2003; *Stevens and Lu,* 2009; *Újvári et al.*, 2010; *Lambert et al.*, 2015], there have been large and systematic variations in dust loading during past glacial–interglacial cycles with dust concentrations during the Last Glacial Maximum (LGM, 19–26 ka) being an order of magnitude higher than during the Holocene [*Fuhrer et al.*, 1999; *Ruth et al.*, 2003; *Fischer et al.*, 2007; *Albani et al.,* 2015]. The possible reasons for enhanced dust flux include increased

wind speeds, reduced strength of the hydrological cycle, expansion of dust source areas, and the physiological effects of low atmospheric CO_2 concentration on terrestrial plant productivity [*Yung et al.*, 1996; *Harrison et al.*, 2001; *Tegen*, 2003]. Aeolian dust has long been recognized as an important tracer for large-scale atmospheric circulation. Since ice core dust is purely aeolian in origin, discrimination of its potential source region(s) would contribute to a better understanding of past dust activity and climatic/environmental causes. Furthermore, ice core dust source information provides critical experimental constraints for model simulations of past atmospheric circulation patterns [*Svensson et al.*, 2000; *Bory et al.*, 2002].

Previous studies on the clay mineralogical and $^{87}Sr/^{86}Sr$ and $^{143}Nd/^{144}Nd$ isotopic compositions of dust in the GISP2 and GRIP ice cores and potential source area (PSA) samples by *Biscaye et al.* [1997] and *Svensson et al.* [2000] suggest that last glacial dust in central Greenland ice cores likely originated from Asia. The Sr–Nd isotopic signature of Greenland ice core dust has been explained as binary mixtures of Chinese/Asian dust and circum-Pacific volcanic material, while both N-America and the Sahara were eliminated as PSAs because of clay mineralogical and Sr–Nd isotopic considerations [*Biscaye et al.*, 1997; *Svensson et al.*, 2000]. This hypothesis of Asian sources of mineral dust has become the prevailing current paradigm for Greenland dust source and informs climate models and reconstructions over past dust dynamics and atmospheric conditions during the last glacial period.

However, *Svensson et al.* [2000] noted that important dust source areas may exist from which no PSA samples were analyzed so far, while some other studies have suggested a different or more complicated picture for Greenland dust sources. *Burton et al.* [2007] found less radiogenic Sr isotopic signatures in LGM dust from the GRIP ice core compared to those published by *Biscaye et al.* [1997] and *Svensson et al.* [2000], and concluded that the

composition of dust transported to Greenland in cold periods is influenced by remote sources like the Gobi or Sahara deserts. A model simulation by *Werner et al.* [2002] suggests that a combination of Caspian Sea–Asian sources accounted for 42% of the total central Greenland dust flux during the LGM, but they emphasize that other sources could also make a significant contribution to the Greenland dust deposition. At the same time, *Aleinikoff et al.* [2008] raise the possibility of North American dust transport to Greenland based on Pb isotopic data of detrital K-feldspars from loess. Model simulations by *Mahowald et al.* [2006] suggest that most of the dust deposited at Greenland could come from sources in the continental U.S., Alaska or Siberia, while in their most recent study, *Mahowald et al.* [2011] simulate both East Asian and Alaskan sources for LGM dust in the GRIP ice core. More recently, *Újvári et al.* [2012] revealed that Sr–Nd isotopic compositions of <5 μm grains of Hungarian LGM loess samples in East Central Europe partly overlap with those of coeval dust samples from the GISP2 and GRIP ice cores. These inconsistencies mean it is now critical to systematically test between the various possible dust sources relevant for Greenland during the last glacial period.

Here we present new clay mineralogical and $^{87}Sr/^{86}Sr$, $^{143}Nd/^{144}Nd$ and $^{176}Hf/^{177}Hf$ isotopic data from fine separates (<10 μm) of eleven LGM loess samples collected around the Northern Hemisphere (Table S1) and compare them to existing LGM Greenland ice core dust data (see Fig. 1 for position of new and published samples used in the analysis). Based on this new data and the published evidence we demonstrate that there are two equally plausible explanations for the origin of last glacial mineral dust recovered from the GISP2/GRIP ice cores. We emphasize that currently no unique source discrimination is possible using both the published and our new data. This underscores the urgent need to reconsider a wider range of possible Greenland dust sources, incorporate this source uncertainty in modeling, and also to identify more diagnostic dust tracers.

2. Material and Methods

Fine (<10 μm) separates of Northern Hemisphere loess sediments were used as PSA samples in this study. All the details of sampling, pretreatments, size separations and clay mineralogical as well as Sr–Nd–Hf isotopic measurements are given in the Supplementary Information file associated with this paper.

3. Results and Discussion

3.1. Clay mineralogical constraints on possible dust sources

Clay mineralogy is a potentially useful tracer of ice core dust provenance as its distribution on the continents is a first-order function of weathering, itself largely a function of climate [*Biscaye et al.,* 1997]. Several clay and other trace mineral distributions are latitude dependent. The most sensitive indicator of this latitude dependency is the kaolinite to chlorite (K/C) ratio [*Biscaye,* 1965], which is an indication of the relative intensities of chemical to physical weathering processes. In a tropical climate we would expect the K/C ratio to be >1–2 [*Scheuvens et al.,* 2013], whereas in a boreal climate it is <0.5–1 [*Griffin et al.,* 1968]. Beyond latitude-indicating species, any source area has a characteristic spectrum of clay minerals, partly reflecting local lithology, climate and drainage characteristics. Source area discrimination is therefore a matter of comparing relative abundances of an entire suite of minerals, some of which may be diagnostic, while others are conversely too common across possible source areas and thus non-characteristic [*Biscaye et al.,* 1997].

In our combined new and literature-based dataset, the K/C ratios of European and Alaskan loess deposits, and some Chinese loess samples overlap with those of last glacial Greenland dust (0.3–0.8; Fig. 2). Only N-American PSAs exhibit much higher K/C ratios (>3.6; Table S2), primarily because of extremely low chlorite contents found in Nebraska loess. In terms of

content, all the PSA samples analyzed so far have lower kaolinite contents than Greenland dust, except for the Alaskan loess. While the illite contents of Alaskan, Central European and Siberian loess samples are in the same range as Greenland LGM dust (40–60 %), some Chinese loess samples reveal higher illite contents (Fig. 2; Table S2). Ice core dust samples are poor in smectite (2–5%) similar to Chinese, Siberian and Alaskan PSAs (Fig. 2; Table S2, and *Svensson et al.,* [2000]). Central/East Central (C/EC) European loess by contrast has higher smectite contents (20–30%), while Nebraska loess was found extremely rich in smectite (except for Jud).

Based on clay mineralogy alone, only the continental US PSAs with very high K/C ratios and extremely high smectite contents can be excluded as potential sources. Alaskan and Chinese loess samples seem to be the best candidates in terms of clay mineral compositions, although Chinese loess has higher illite and lower kaolinite contents and K/C ratios than Greenland dust in our datasets. Siberian and C/EC European loess deposits are still considered potential sources, although the former has slightly lower kaolinite, while the latter has higher smectite contents. A crucial problem in discriminating the provenance of Greenland dust is that relatively little is known about the impact of long-range transport on mineralogical compositions. While there is some evidence that the illite/kaolinite (I/K) ratio remains stable during emission and long-range transport of mineral aerosol [*Glaccum and Prospero,* 1980; *Caquineau et al.,* 1998], smectite tends to agglutinate during transport due to its high hygroscopic capacity [*Singer et al.,* 2004]. The very fine grain size of smectite at emission and its tendency to form aggregates during atmospheric transport result in a fractionation effect [*Tomadin et al.,* 1989; *Scheuvens et al.,* 2013]. While smectite occurrence exhibits a latitudinal dependence in atmospheric dust samples collected along the western coast of Africa [*Stuut et al.,* 2005], *Chester et al.* [1971] found high variability in smectite contents (2–43 wt.%), and attributed this as likely resulting from physical fractionation processes during

emission, transport and deposition, as well as heterogeneous smectite contents in the source sediments [*Schütz and Sebert,* 1987]. Thus, without a deeper understanding of this fractionation and source heterogeneity, the usefulness of smectite as a source marker remains uncertain [*Scheuvens et al.,* 2013], particularly in source discriminations based on loess samples exhibiting relatively little (10–20%) inter-regional differences in smectite contents. At the same time, large and significant differences in smectite contents can still to some extent be considered source-diagnostic, in particular if other clay mineralogical parameters (e.g. K/C ratio) are also divergent. *Aleinikoff et al.* [2008] argued that higher smectite contents in continental US dust deposits do not necessarily rule these out as sources for central Greenland last glacial dust, as smectite in Nebraska loess source rocks forms hard-to-remove coatings on larger grains that would drop out near the source. Nevertheless, it seems still unlikely that fractionation processes during transport would lead to 60-70 % smectite depletion for the Nebraska loess, which would be required for it to match the smectite contents of LGM Greenland dust. In any case, while the interpretation of smectite content is somewhat ambiguous, neither the very low kaolinite and chlorite contents nor the high K/C ratios favor continental US sources.

3.2. Sr–Nd isotopic compositions and mixing models: two plausible explanations

$^{87}Sr/^{86}Sr$ isotopic ratios cover a range from 0.715178 to 0.722874, with the Nebraska loess exhibiting the least radiogenic and Chinese loess the most radiogenic Sr isotopic compositions (Table S2). $^{143}Nd/^{144}Nd$ isotopic ratios were found in a relatively narrow range from 0.512044 to 0.512160 ($\varepsilon_{Nd}(0)$: –11.4 to –9.2; Table S3; for the definition of $\varepsilon_{Nd}(0)$ see the Supplementary Information). Less radiogenic Nd isotopic compositions are characteristic for one of the Nebraska and Siberian loess samples. In Sr–Nd isotopic space, the C/EC European loess deposits most overlap with the last glacial Greenland dust samples (Fig. 3a,b), and while

200 the Nebraska loess is slightly less radiogenic in Sr–Nd isotopes, and Chinese loess reveals a
201 slightly more radiogenic Sr isotopic signature (Fig. 3a,b), both are also close to Greenland
202 dust composition. However, neither of the Chinese-Mongolian desert sources overlap in Sr–
203 Nd isotopic compositions with those of Greenland LGM dust [*Chen et al.,* 2007; *Zhao et al.,*
204 2015], except for the Northern Mongolia Plateau clay (<2 μm) separates. As such, it is also
205 plausible that this latter region may have provided mineral dust to Greenland during the last
206 glacial. However, as explained below, we propose that two potential dominant dust source
207 regions can best account for the new data here, and the published work: China and C/EC
208 Europe. Furthermore, we argue that neither of these PSAs can be distinguished as the
209 dominant LGM Greenland dust source based on these and all published data.
210 A complicating factor in the analysis is that although the sampled GISP2 and GRIP ice core
211 sections were free of volcanic markers, a low amount of volcanogenic component cannot be
212 entirely excluded because of the weak electric conductivity signal in alkaline ice [*Hammer et*
213 *al.,* 1997; *Svensson et al.,* 2000]. Therefore, both *Biscaye et al.* [1997] and *Svensson et al.*
214 [2000] considered a weak (up to ~10%) contribution from circum-Pacific volcanic sources
215 situated upwind of Greenland. Considering that, as found by *Svensson et al.* [2000], an
216 admixture of 90–10 % from Chinese loess and circum-Pacific volcanic material would
217 account for the Sr–Nd isotopic ratios of central Greenland LGM dust (Fig. 3a,b; gray mixing
218 hyperbola). However, at the same time *Svensson et al.* [2000] argue that it seems unlikely that
219 more than half of their samples contain almost the same fraction of volcanic material, and the
220 low inter-sample Sr isotopic variability implies an insignificant volcanic component.
221 Considering this negligible volcanic input, our new Sr–Nd isotopic dataset from PSAs offers a
222 potential alternative model involving C/EC Europe that is capable of explaining the ice core
223 dust Sr–Nd isotopic compositions. A mixture of a zero to 5% volcanic component and 95–
224 100% C/EC European loess would yield the Sr–Nd isotopic ratios of LGM dust in GISP2 and

GRIP (Fig. 3a,b; black mixing hyperbola). Furthermore, in this model the isotopic composition of C/EC European loess itself explains the $^{87}Sr/^{86}Sr$ and $^{143}Nd/^{144}Nd$ isotopic ratios of ice core dust without invoking a volcanic source.

This latter C/EC European dust source hypothesis would, however, require a direct dust transport route from Europe to Greenland. Such a route, as modeled for the LGM by *Andersen et al.* [1998], is through strong northward advection over the central part of Eurasia, across the Arctic Ocean, and around a persistent low pressure system in the Baffin Bay. This meridional path over the Arctic Ocean was found in an air mass trajectory analysis to Summit, Greenland for the present-day [*Kahl et al.,* 1997], albeit with a rare occurrence. In that study though, N-America was found to be an important source for all seasons, while for wintertime 67% of all 10-day trajectories reached back to Asia/Europe. It follows from this study that Asia is also among the most important sources today and this might be true for the LGM, too. Indeed, some LGM atmospheric simulations favor Asian sources for last glacial dust over central Greenland [*Reader et al.,* 1999, *Werner et al.,* 2002; *Mahowald et al.,* 2011], while others suggest dust transport from glaciogenic/non-glaciogenic sources in the continental US, Alaska or Siberia [*Mahowald et al.,* 2006].

A further line of evidence is the origin of volcanic material in Greenland ice. Tephra studies on Greenland ice cores indicate that, beyond a clear dominance of proximal Jan Mayen and Icelandic sources, volcanic ash from the Pacific Arc was repeatedly transported and deposited in Greenland [*Abbott and Davies,* 2012; *Bourne et al.,* 2015a; *Bourne et al.,* 2015b]. Together with this Pacific material, volcanic material from only some Southern European eruptions (Vesuvius, 79 AD and perhaps Santorini, ~1645 BC) can be traced in Greenland ice cores [*Abbott and Davies,* 2012], and neither the Campanian Ignimbrite (~40 ka) nor the Laacher See (~12.9 ka) tephras could be identified in NGRIP and NEEM [*Svensson,* 2012; *Bourne et al.,* 2013]. Out of the numerous N-American eruptions, only the Alaskan White River Ash

(~860 AD) and the Mount Mazama Ash (~7.6 ka) appear in NEEM [*Jensen et al.,* 2012] and GISP2 [*Zdanowicz et al.,* 1999]. This data therefore point to a dominant dust transport pathway from East Asia to Greenland during the last glacial period. As shown above, such a link is supported by the Sr–Nd isotopic signatures of Chinese loess deposits and in general by their clay mineralogy. However, since the illite contents of Chinese loess are by 10–25 % higher than those of ice core dust, some loss during transport may have happened. Although less consistent with tephra records and atmospheric circulation simulations, the C/EC European loess Sr–Nd signatures strongly point to a LGM Greenland dust source in this region. The clay mineral compositions are entirely overlapping, except for smectite, which is present in slightly higher amounts in C/EC European loess than in ice core dust. Nevertheless, these differences are minor (10–20 %, mostly within XRD measurement uncertainties), and some amounts of smectite may have been lost during transport.

While the published and new data here cannot differentiate between an Asian or C/EC European source, we argue that the possibility of a dominant N-American and Siberian dust source to Greenland can be excluded. With regard to published work, sourcing of Greenland material from Alaskan dust was rejected by *Biscaye et al.* [1997] using Sr–Nd isotopes. Indeed, a genetic link between Alaskan and Greenland dust is improbable considering the previously published Sr–Nd isotopic signatures of Yukon loess fine grain separates (0.707–0.71, $\varepsilon_{Nd}(0)$: –4 to 2) [*Zdanowicz et al.,* 2006]. Likewise, the sourcing of Greenland dust from the continental US seems also unlikely based on the clay mineralogy presented here, especially given the very low kaolinite and chlorite contents in Nebraska loess, which could clearly not be enriched en route to Greenland during transport (see above; Fig. 2). Further evidence against the continental US origin comes from the less radiogenic Sr–Nd isotopic ratios of Nebraska loess compared to those of central Greenland LGM dust in the data presented here (Fig. 3). Although few of the samples overlap, the more radiogenic Sr–Nd

isotopic ratios of ice core dust could only be accounted for by mixing Nebraska loess with dust from a source characterized by much more radiogenic Sr–Nd isotopic ratios than the ice core dust. At the same time, any mixture of Nebraska loess with volcanic products would result in much lower $^{87}Sr/^{86}Sr$ isotopic ratios than those of ice core dust. With regards to a possible NE-Siberian origin, this region cannot be excluded as a source based on clay mineralogy. However, the less radiogenic Nd isotopic signature of the Sib200 sample does not support a link to Greenland from this region (Fig. 3a,b; Table S3). Nevertheless, further loess samples should be analyzed to gain insight into the mineralogical and isotopic heterogeneity of these sources.

3.3. Hf isotopes as promising tracers

The ambiguities in source discrimination presented above imply that new approaches are needed to answer the still open question of last glacial ice core dust origin in central Greenland. Hf isotopic analysis on the low amounts of material (0.7–8 mg dust/kg ice) that are usually found in ice cores from the LGM to the Holocene [*Ruth et al.,* 2003] is challenging, but feasible [*Aciego et al.,* 2009]. Here we present some initial Hf isotopic analyses on the <10 μm fraction of LGM loess samples. These data coupled with Nd–Hf isotopic ratios from the recent literature (Fig. 3c) suggest that such efforts are valuable as it is expected that the Hf isotopes will provide more source-diagnostic data.

First, we tested the effect of acid treatment on Hf isotopes, as all of the PSAs were leached using weak acetic acid to remove carbonates (see the Supplementary Information). Since carbonates are not the carriers of Lu and/or Hf, it was expected that the Hf isotopic signatures are not influenced by the acetic acid treatment. Indeed, similarly to Nd isotopes, Hf isotopic ratios do not seem to be affected by weak acetic acid leaching (Table S3).

Second, we analyzed the range of Nd–Hf isotopic data in the samples. As shown in Fig. 3c and Table S3, Nd isotopic compositions ($\varepsilon_{Nd}(0)$) of the three acid treated grain size separates analyzed in this study range from –11.4 to –10, close to the average upper crustal value of –10.3 [*Chauvel et al.,* 2014]. Bulk loess samples from China, Tajikistan and W-Europe have almost the same $\varepsilon_{Nd}(0)$ values as the grain size separates, although with a slightly larger range (Fig. 3c). By contrast, bulk loess $\varepsilon_{Hf}(0)$ values show large variations, and are always much more negative than those from the loess fine grain separates. These much less radiogenic Hf isotopic compositions of the bulk loess are attributed to higher zircon abundances in these samples [*Patchett et al.,* 1984; *Pettke et al.,* 2002; *van de Flierdt et al.,* 2007; *Lupker et al.,* 2010; *Rickli et al.,* 2010; *Garcon et al.,* 2013; *Chauvel et al.,* 2014], meaning these plot around the 'Zircon-bearing sediment array' [*Bayon et al.,* 2009]. Zircon is a refractory heavy mineral with low Lu/Hf ratios [*Hoskin and Schaltegger,* 2003] and thus very unradiogenic $^{176}Hf/^{177}Hf$ isotopic compositions [*Kinny and Maas,* 2003; *Újvári and Klötzli,* 2015], which then also consequently dominate the bulk loess Hf isotopic signal. By contrast, fine grain separates of loess plot between the 'Zircon-free' and 'Clay-sized arrays' (Fig. 3c), demonstrating that they contain little to no zircon and their more radiogenic Hf isotopic compositions are controlled by clay minerals that incorporate/adsorb radiogenic Hf released from higher Lu/Hf phases during incongruent weathering [*van de Flierdt et al.,* 2007; *Bayon et al.,* 2009; *Zhao et al.,* 2014]. In our limited dataset, the Hf isotopic compositions of fine grain separates are found to be strongly correlated with illite contents (Fig. 3d), with the differences in $\varepsilon_{Hf}(0)$ values (–6.5 to –1.8) between samples reaching several ε_{Hf} units. We therefore suggest that in the absence of zircons, the Hf isotopic compositions likely reflect the different proportions of clay minerals characteristic for each loess region on the Northern Hemisphere, in particular illite. In our dataset these proportions appear to be sufficiently different in the fine grain PSA data to enable discrimination. Further, the Hf isotopic

composition of very fine mineral dust in Greenland is also expected to be clay mineralogy dependent because of zircon depletion and fallout during long atmospheric transport [*Aarons et al., 2013*]. As such, it is believed that through Hf isotopes a better understanding can be gained concerning Greenland dust sources, although for this to be achieved, further clay mineralogy and Hf isotopic data are needed to better understand the first-order clay mineralogical controls on Hf isotopic signatures of fine dust.

4. Conclusions

Clay mineralogy and Sr–Nd isotopic ratios of grain size separates (<10 μm) of Northern Hemisphere loess samples demonstrate that two plausible scenarios exist for the origin of last glacial mineral dust found in the GISP2 and GRIP ice cores. While the Northern Mongolia and Chinese Loess Plateau deposits still appear to be the most likely dust sources, the Sr–Nd isotopic compositions of LGM ice core dust can readily be explained by major contributions from C/EC European loess deposits too. Clay mineralogical compositions do not seem to contradict this hypothesis. At the same time, the clay mineralogy coupled with the less radiogenic Sr–Nd isotopic signatures of Nebraska loess do not support a sourcing of Greenland dust from major continental N-American glacial dust emitting regions. Likewise, a NE-Siberian origin also seems less likely based on the Nd isotopic ratio of a single sample, although further data would be needed from dust samples of both regions. Based on initial Hf isotope analyses of fine separates of three loess samples, an apparent dependence of Hf isotopic signatures on the relative proportions of radiogenic clay minerals (primarily illite) can be seen, as these fine dust fractions seem to be zircon-free. The observed difference between major potential source regions in $^{176}Hf/^{177}Hf$ that reach several ε_{Hf} units and the first-order clay mineralogy dependence of Hf isotopic signatures means there is strong potential for

distinguishing between the two hypothesized Greenland dust sources using Hf isotopes. For this, however, Hf isotopic measurements on Greenland ice core dust samples are required.

Acknowledgments

This work has been funded by the Director-General' allowance of the MTA Research Centre for Astronomy and Earth Sciences, and a post doc project from the NKFIH to GÚ (OTKA PD-108639). Additional financial support provided by the Bolyai János Research Scholarship of the Hungarian Academy of Sciences to GÚ (BO/00326/15/10) is gratefully acknowledged. Constructive comments by Joe Mason and an anonymous reviewer improved the quality of this paper. Editorial handling by Kim Cobb is appreciated. The data used are listed in the references and the Supplementary Information file.

Author contributions

GÚ designed the study, performed the field work and sampling in Hungary. MRS, MG, GLBW, TS, SBM, and MZ did field work and sampling in the US, Germany, China, Serbia and Siberia and provided samples. GÚ and JK performed laboratory preparations (wet sedimentation, acid treatment), and laser diffraction measurements. NT did the XRD analyses, while UK and CM performed the Sr-Nd-Hf isotopic analyses in Vienna, London and Leeds. GÚ wrote the paper with the active participation of TS and AS. All authors contributed to the discussion/interpretation of results.

373 **References**

374 Aarons, S.M., S.M. Aciego, and J.D. Gleason (2013), Variable Hf-Sr-Nd radiogenic isotopic
375 compositions in a Saharan dust storm over the Atlantic: Implications for dust flux to
376 oceans, ice sheets and the terrestrial biosphere, *Chem. Geol.,* 349–350, 18–26.

377 Abbott, P.M., and S.M. Davies, S.M (2012), Volcanism and the Greenland ice-cores: the
378 tephra record, *Earth-Sci Rev.,* 115, 173–191.

379 Aciego, S.M., B. Bourdon, M. Lupker, and J. Rickli (2009), A new procedure for separating
380 and measuring radiogenic isotopes (U, Th, Pa, Ra, Sr, Nd and Hf) in ice cores, *Chem.*
381 *Geol.,* 266, 194–204.

382 Albani, S., N.M. Mahowald, G. Winckler, R.F. Anderson, L.I. Bradtmiller, B. Delmonte, R.
383 François, M. Goman, N.G. Heavens, P.P. Hesse, S.A. Hovan, S.G. Kang, K.E. Kohfeld,
384 H. Lu, V. Maggi, J.A. Mason, P.A. Mayewski, D. McGee, X. Miao, B.L. Otto-Bliesner,
385 A.T. Perry, A. Pourmand, H.M. Roberts, N. Rosenbloom, T. Stevens, and J. Sun (2015),
386 Twelve thousand years of dust: the Holocene global dust cycle constrained by natural
387 archives, *Clim. Past,* 11, 869–903.

388 Albrecht, B.A. (1989), Aerosols, cloud microphysics, and fractional cloudiness, *Science,* 245,
389 1227–1230.

390 Aleinikoff, J.N., D.R. Muhs, E.A. Bettis III, W.C. Johnson, C.M. Fanning, and R. Benton
391 (2008), Isotopic evidence for the diversity of late Quaternary loess in Nebraska:
392 glaciogenic and nonglaciogenic sources, *Geol. Soc. Am. Bull.,* 120, 1362–1377.

393 Andersen, K.K., A. Armengaud, C. Genthon (1998), Atmospheric dust under glacial and
394 interglacial conditions, *Geophys. Res. Lett.,* 25, 2281–2284.

395 Andreae, M.O., and D. Rosenfeld (2008), Aerosol-cloud-precipitation interactions. Part 1.
396 The nature and sources of cloud-active aerosols, *Earth-Sci. Rev.,* 89,13–41.

Archer, D., A. Winguth, D. Lea, and N. Mahowald (1998), What caused the glacial-interglacial atmospheric pCO2 cycles?, *Rev. Geophys.,* 38, 159–189.

Bayon, G., K.W. Burton, G. Soulet, N. Vigier, B. Dennielou, J. Etoubleau, E. Ponzevera, C. R. German, and R.W. Nesbitt (2009), Hf and Nd isotopes in marine sediments: Constraints on global silicate weathering, *Earth Planet. Sci. Lett.,* 277, 318–326.

Biscaye, P.E. (1965), Mineralogy and sedimentation of recent deep-sea clay in the Atlantic Ocean and adjacent seas and oceans, *Geol. Soc. Am. Bull.,* 76, 803–832.

Biscaye, P.E., F.E. Grousset, M. Revel, S. Van der Gaast, G.A. Zielinski, A. Vaars, and G. Kukla (1997), Asian provenance of glacial dust (stage 2) in the Greenland Ice Sheet Project 2 Ice Core, Summit, Greenland, *J. Geophys. Res.,* 102, 26765–26781.

Bory, A.J.-M., P.E. Biscaye, A. Svensson, and F.E. Grousset (2002), Seasonal variability in the origin of recent atmospheric mineral dust at NorthGRIP, Greenlan,. *Earth Planet. Sc. Lett.* 196, 123–134.

Bourne, A.J., S.M. Davies, P.M. Abbott, S.O. Rasmussen, J.P. Steffensen, and A. Svensson (2013), Revisiting the Faroe Marine Ash Zone III in two Greenland ice cores: implications for marine-ice correlations, *J. Quat. Sci.,* 28, 641–646.

Bourne, A.J., E. Cook, P.M. Abbott, I.K. Seierstad, J.P. Steffensen, A. Svensson, H. Fischer, S. Schüpbach, and S.M. Davies (2015a), A tephra lattice for Greenland and a reconstruction of volcanic events spanning 25-45 ka b2k, *Quat. Sci. Rev.,* 118, 122–141.

Bourne, A.J., P.M. Abbott, E. Cook, S.M. Davies, A.N. Derkachev, N.J.P. Pearce, V. Ponomareva, M.V. Portnyagin, and A. Svensson (2015b), Repeated long-range ash transport from Pacific arc volcanic sources: evidence from the Greenland ice-cores, in XIX INQUA Congress Program Book, edited by Y. Saito et al., S05–04, T00932.

420 Burton, G.R., K.J.R. Rosman, J.-P. Candelone, L.J. Burn, C.F. Boutron, and S. Hong (2007),
421 The impact of climatic conditions on Pb and Sr isotopic ratios found in Greenland ice, 7
422 – 150 ky BP, *Earth Planet. Sc. Lett.,* 259, 557–566.
423 Caquineau, S., A. Gaudichet, L. Gomes, M.C. Magonthier, and B. Chatenet (1998), Saharan
424 dust: clay ratio as a relevant tracer to assess the origin of soil derived aerosols, *Geophys.*
425 *Res. Lett.,* 25, 983–986.
426 Chauvel, C., M. Garcon, S. Bureau, A. Besnault, B-M. Jahn, Z. Ding (2014), Constraints from
427 loess on the Hf-Nd isotopic composition of the upper continental crust, *Earth Planet.*
428 *Sci. Lett.,* 388, 48–58.
429 Chen, J., G. Li, J. Yang, W. Rao, H. Lu, W. Balsam, Y. Sun, and J. Ji (2007), Nd and Sr
430 isotopic characteristics of Chinese deserts: implications for the provenances of Asian
431 dust, *Geochim. Cosmochim. Ac.,* 71, 3904–3914.
432 Derbyshire, E. (2003), Loess, and the Dust Indicators and Records of Terrestrial and Marine
433 Palaeoenvironments (DIRTMAP) database, *Quaternary Sci. Rev.,* 22, 1813–1819.
434 Duce, R.A., and N.W. Tindale (1991), Atmospheric transport of iron and its deposition in the
435 ocean, *Limnol. Oceanogr.,* 36, 1715–1726.
436 Falkowski, P.G., R.T. Barber, and V. Smetacek (1998), Biogeochemical controls and
437 feedbacks on ocean primary production, *Science,* 281, 200–206.
438 Feng, J.-L., L.-P. Zhu, X.-L. Zhen, Z.-G. Hu (2009), Grain size effect on Sr and Nd isotopic
439 compositions in eolian dust: Implications for tracing dust provenance and Nd model
440 age, *Geochem. J.,* 43, 123–131.
441 Fischer, H., M.-L. Siggaard-Andersen, U. Ruth, R. Röthlisberger, and E. Wolff (2007),
442 Glacial/interglacial changes in mineral dust and sea-salt records in polar ice cores:
443 sources, transport, and deposition, *Rev. Geophys.,* 45, RG1002, doi:
444 10.1029/2005RG000192.

445 Fuhrer, K., E.W. Wolff, and S.J. Johnsen (1999), Timescales for dust variability in the
446 Greenland Ice Core Project (GRIP) ice core in the last 100,000 years, *J. Geophys. Res.,*
447 104, 31043–31052.
448 Garcon, M., C. Chauvel, C. France-Lanord, P. Huyghe, and J. Lavé (2013), Continental
449 sedimentary processes decouple Nd and Hf isotopes, *Geochim. Cosmochim. Ac.*, 121,
450 177–195.
451 George, R., S. Turner, C. Hawkesworth, J. Morris, C. Nye, J. Ryan, and S-H. Zheng (2003),
452 Melting processes and fluid and sediment transport rates along the Alaska-Aleutian arc
453 from an integrated U-Th-Ra-Be isotope study, *J. Geophys. Res.,* 108, B5, 2252,
454 doi:10.1029/2002JB001916.
455 Glaccum, R.A., and J.M. Prospero (1980), Saharan aerosols over the tropical north Atlantic
456 —mineralogy, *Mar. Geol.,* 37, 295–321.
457 Griffin, J.J., and E.D. Goldberg (1968), Clay mineral distribution in the world ocean, *Deep*
458 *Sea Res.,* 15, 433–459.
459 Grousset, F.E., P.E. Biscaye, A. Zindler, J.M. Prospero, and R. Chester (1988), Neodymium
460 isotopes as tracers in marine sediments and aerosols: North Atlantic, *Earth Planet. Sc.*
461 *Lett.,* 87, 367–378.
462 Grousset, F.E., P. Rognon, G. Coudé-Gaussen, Ph. Pédemay (1992), Origins of peri-Saharan
463 dust deposits traced by their Nd and Sr isotopic composition, *Palaeogeogr. Palaeocl.,*
464 93, 203–212.
465 Grousset, F.E., M. Parra, A. Bory, P. Martinez, P. Bertrand, G. Shimmield, and R. Ellam
466 (1998), Saharan wind regimes traced by the Sr–Nd isotopic composition of the tropical
467 Atlantic sediments: last glacial maximum vs. today, *Quaternary Sci. Rev.,* 17, 395–409.
468 Hammer,C.U., H.B. Clausen, and C.C. Langway Jr (1997), 50,000 years of recorded global
469 volcanism, *Clim. Change,* 35, 1–15.

Harrison, S.P., K.E. Kohfeld, C. Roelandt, and T. Claquin (2001), The role of dust in climate changes today, at the last glacial maximum and in the future, *Earth-Sci. Rev.,* 54, 43–80.

Hoskin, P.W.O., and U. Schaltegger (2003), The composition of zircon and igneous and metamorphic petrogenesis, in Zircon, Reviews in Mineralogy and Geochemistry, vol. 53, edited by J.M. Hanchar and P.W.O. Hoskin, pp. 27–62.

Jensen, B.J.L., S. Pyne-O'Donnell, G. Plunkett, D.G. Froese, P.D.M. Hughes, M. Sigl, J.R. McConnell, M.J. Amesbury, P.G. Blackwell, C. van den Bogaard, C.E. Buck, D.J. Charman, J.J. Clague, V.A. Hall, J. Koch, H. Mackay, G. Mallon, L. McColl, and J.R. Pilcher (2014), Transatlantic distribution of the Alaskan White River Ash, *Geology,* 42, 875–878.

Kahl, J.D.W., D.A. Martinez, H. Kuhns, C.I. Davidson, J-L. Jaffrezo, and J.M. Harris (1997), Air mass trajectories to Summit, Greenland: A 44-year climatology and some episodic events. *J. Geophys. Res.,* 102, 26861–26875.

Kepezhinskas, P. F. McDermott, M.J. Defant, A. Hochstaedter, M.S. Drummond, C.J. Hawkesworth, A. Koloskov, R.C. Maury, H. Bellon (1997), Trace element and Sr-Nd-Pb isotopic constraints on a three-component model of Kamchatka Arc petrogenesis, *Geochim. Cosmochim. Ac.,* 61, 577–600.

Kinny, P.D., and R. Maas (2003), Lu–Hf and Sm–Nd isotope systems in zircon, in Zircon, Reviews in Mineralogy and Geochemistry, vol 53, edited by J.M. Hanchar and P.W.O. Hoskin PWO, pp. 327–341.

Kohfeld, K.E., and S.P. Harrison (2001), DIRTMAP: the geological record of dust, *Earth-Sci. Rev.,* 54, 81–114.

Lambert, F., B. Delmonte, J.R. Petit, M. Bigler, P.R. Kaufmann, M.A. Hutterli, T.F. Stocker, U. Ruth, J.P. Steffensen, and V. Maggi (2008), Dusteclimate couplings over the past 800,000 years from the EPICA Dome C ice core, *Nature,* 452, 616–619.

Lambert, F., A. Tagliabue, G. Shaffer, F. Lamy, G. Winckler, L. Farias, L. Gallardo, and R. De Pol-Holz (2015), Dust fluxes and iron fertilization in Holocene and Last Glacial Maximum climates, *Geophys. Res. Lett.,* 42, doi:10.1002/2015GL064250.

Liao, H., and J.H. Seinfeld (1998), Radiative forcing by mineral dust aerosols: sensitivity to key variables, *J. Geophys. Res.,* 103, 31637–31645.

Lupker, M., S.M. Aciego, B. Bourdon, J. Schwander, and T.F. Stocker (2010), Isotopic tracing (Sr, Nd, U and Hf) of continental and marine aerosols in an 18th century section of the Dye-3 ice core (Greenland), *Earth Planet. Sc. Lett.,* 295, 277–286.

Mahowald, N.M., A.R. Baker, G. Bergametti, N. Brooks, R.A. Duce, T.D. Jickells, N. Kubilay, J.M. Prospero, and I. Tegen (2005), Atmospheric global dust cycle and iron inputs to the ocean, *Global Biogeochem. Cy.,* 19, GB4025. doi:10.1029/2004GB002402.

Mahowald, N.M., D.R. Muhs, S. Levis, P.J. Rasch, M. Yoshioka, C.S. Zender, and C. Luo (2006), Change in atmospheric mineral aerosols in response to climate: last glacial period, preindustrial, modern, and doubled carbon dioxide climates, *J. Geophys. Res.,* 111, D10202.

Mahowald, N.M., S. Albani, S. Engelstaedter, G. Winckler, and M. Goman (2011), Model insight into glacial–interglacial paleodust records. *Quaternary Sci. Rev.,* 30, 832–854.

Martin, J.H. (1990), Glacial - interglacial CO2 change: the iron hypothesis, *Palaeoceanography,* 5, 1–13.

Patchett P.J., W.M. White, H. Feldmann, S. Kielinczuk, and A.W. Hofmann (1984), Hafnium/rare earth element fractionation in the sedimentary system and crustal recycling into the Earth's mantle, *Earth Planet. Sci. Lett. 69,* 365–378.

518 Pettke T., D.-C. Lee, A.N. Halliday, and D.K. Rea (2002), Radiogenic Hf isotopic
519 compositions of continental eolian dust from Asia, its variability and its implications for
520 seawater Hf, *Earth Planet. Sci. Lett.*, 202, 453–464.
521 Porter, S.C., and Z.S. An (1995), Correlation between climate events in the North Atlantic and
522 China during the last glaciation, *Nature,* 375, 305–308.
523 Reader, M.C., I. Fung, and N. McFarlane (1999), The mineral dust aerosol cycle during the
524 Last Glacial Maximum, *J. Geophys. Res.,* 104, 9381–9398.
525 Rickli J., M. Frank, A.R. Baker, S. Aciego, G. de Souza, R.B. Georg, and A.N. Halliday
526 (2010), Hafnium and neodymium isotopes in surface waters of the eastern Atlantic
527 Ocean: implications for sources and inputs of trace metals to the ocean, *Geochim.*
528 *Cosmochim. Ac.,* 74, 540–557.
529 Ruth, U., D. Wagenbach, J.P. Steffensen, and M. Bigler (2003), Continuous record of
530 microparticle concentration and size distribution in the central Greenland NGRIP ice
531 core during the last glacial period, *J. Geophys. Res.,* 108, D3, 4098, doi:
532 10.1029/2002JD002376.
533 Scheuvens, D., L. Schütz, K. Kandler, M. Ebert, and S. Weinbruch (2013), Bulk composition
534 of northern African dust and its source sediments — A compilation, *Earth-Sci. Rev.,*
535 116, 170–194.
536 Schütz, L., and M. Sebert (1987), Mineral aerosols and source identification, *J. Aerosol Sci.,*
537 18, 1–10.
538 Steffensen, J.P. (1997), The size distribution of microparticles from selected segments of the
539 Greenland Ice Core Project ice core representing different climate periods, *J. Geophys.*
540 *Res.,* 102, 26755–26763.

541 Stevens, T., and H. Lu (2009), Optically stimulated luminescence dating as a tool for
542 calculating sedimentation rates in Chinese loess: comparisons with grain-size records.
543 *Sedimentology,* 56, 911–934.
544 Stuut, J.B., M. Zabel, V. Ratmeyer, P. Helmke, E. Schefuß, G. Lavik, and R. Schneider
545 (2005), Provenance of present-day eolian dust collected off NW Africa, *J. Geophys.*
546 *Res.,* 110, D04202. http://dx.doi.org/10.1029/2004JD005161.
547 Svensson, A. (2012), The missing tephra horizons in the Greenland ice cores, in XVIII
548 INQUA Congress: Collection of Abstracts, edited by C. Schlüchter, and J. Nietlispach,
549 *Quat. Int.,* 279/280, p. 478.
550 Svensson, A., P.E. Biscaye, and F.E. Grousset (2000), Characterization of late glacial
551 continental dust in the Greenland Ice Core Project ice core, *J. Geophys. Res.,* 105,
552 4637–4656.
553 Tegen, I. (2003), Modeling the mineral dust aerosol cycle in the climate system, *Quaternary*
554 *Sci. Rev.* 22, 1821–1834.
555 Tegen, I., and A.A. Lacis (1996), Modeling of particle size distribution and its influence on
556 the radiative properties of mineral dust aerosol, *J. Geophys. Res.,* 101, 19237–19244.
557 Thompson, L.G., and E. Mosley-Thompson (1981), Microparticle concentration variations
558 linked with climatic change: evidence from polar ice cores, *Science,* 212, 812–815.
559 Tomadin, L., G. Cesari, S. Fuzzi, V. Landuzzi, R. Lenaz, A. Lobietti, P. Mandrioli, M.
560 Mariotti, A. Mazzucotelli, and R. Vannucci (1989), Eolian dust collected in springtime
561 (1979 and 1984 years) at the seawater–air interface of the Northern Red Sea, in
562 Palaeoclimatology and Palaeometeorology: Modern and Past Patterns of Global
563 Atmospheric Transport, NATO ASI Ser. C, vol. 282, edited by M. Leinen and M.
564 Sarnthein, pp. 283–310, Kluwer Academic Publishers, Dordrecht, The Netherlands.

565 Újvári, G., and U. Klötzli (2015) U–Pb ages and Hf isotopic composition of zircons in
566 Austrian last glacial loess: constraints on heavy mineral sources and sediment transport
567 pathways, *Int. J. Earth Sci.,* 104, 1365–1385.
568 Újvári, G., J. Kovács, Gy. Varga, B. Raucsik, and S.B. Markovic (2010), Dust flux estimates
569 for the Last Glacial Period in East Central Europe based on terrestrial records of loess
570 deposits: a review, *Quaternary Sci. Rev.,* 29, 3157–3166.
571 Újvári, G., A. Varga, F.C. Ramos, J. Kovács, T. Németh, and T. Stevens (2012), Evaluating
572 the use of clay mineralogy, Sr–Nd isotopes and zircon U–Pb ages in tracking dust
573 provenance: An example from loess of the Carpathian Basin, *Chem. Geol.,* 304–305,
574 83–96.
575 van de Flierdt T., S.L. Goldstein, S.R. Hemming, M. Roy, M. Frank, and A.N. Halliday
576 (2007), Global neodymium–hafnium isotope systematics—revisited, *Earth Planet. Sci.*
577 *Lett.*, 259, 432–441.
578 Vervoort, J.D., T. Plank, and J. Prytulak (2011), The Hf-Nd isotopic composition of marine
579 sediments, *Geochim. Cosmochim. Ac.,* 75, 5903–5926.
580 Werner, M., I. Tegen, S. Harrison, K. Kohfeld, I.C. Prentice, Y. Balkanski, H. Rodhe, and C.
581 Roelandt (2002), Seasonal and interannual variability of the mineral dust cycle under
582 present and glacial climate conditions, *J. Geophys. Res.,* 107, 4744,
583 doi:10.1029/2002JD002365.
584 Winckler, G., R.F. Anderson, M.Q. Fleischer, D. McGee, and N. Mahowald (2008), Covariant
585 Glacial-interglacial dust fluxes in the Equatorial Pacific and Antarctica, *Science,* 320,
586 93-96, doi: 10.1126/science.1150595.
587 Yin, Y., S. Wurzler, Z. Levin, and T.G. Reisin (2002), Interactions of mineral dust particles
588 and clouds: effects on precipitation and cloud optical properties, *J. Geophys. Res.,* 107,
589 4724. doi:10.1029/2001JD001544.

590 Yung, Y.L., T. Lee, C.-H. Wang, Y.-T. Shieh (1996), Dust: a diagnostic of the hydrological
591 cycle during the Last Glacial Maximum, *Science,* 271, 962–963.
592 Zdanowicz, C.M., G.A. Zielinski, and M.S. Germani (1999), Mount Mazama eruption:
593 calendrical age verified and atmospheric impact assessed, *Geology,* 27, 621–624.
594 Zdanowicz, C., G. Hall, J. Vaive, Y. Amelin, J. Percival, I. Girard, P. Biscaye, and A. Bory
595 (2006), Asian dustfall in the St. Elias Mountains, Yukon, Canada, *Geochim.*
596 *Cosmochim. Ac.,* 70, 3493–3507.
597 Zhao, W., Y. Sun, W. Balsam, H. Lu, L. Liu, J. Chen, and J. Ji (2014), Hf–Nd isotopic
598 variability in mineral dust from Chinese and Mongolian deserts: Implications for
599 sources and dispersal, *Sci. Rep.*, 4, 5837, doi:10.1038/srep05837.
600 Zhao, W., Y. Sun, W. Balsam, L. Zeng, H. Lu, K. Otgonbayar, and J. Ji (2015), Clay-sized
601 Hf-Nd-Sr isotopic composition of Mongolian dust as a fingerprint for regional to
602 hemispherical transport, Geophys. Res. Lett., 42, doi:10.1002/2015GL064357.
603

604 **Figure captions**

605 **Figure 1.** Location of ice cores in Greenland and potential source area (PSA) samples around
606 the Northern Hemisphere. Black dots denote PSAs analyzed by *Biscaye et al.* [1997] and
607 *Svensson et al.* [2000]: 1-2. Moose Mts., AK, USA; 3. Pullman, WA, USA; 4. Pancake
608 Hollow, IL, USA; 5-7. Gobi desert; 8. Weinan, China; 9. Luochuan, China; 10. Yulin, China;
609 11. Muzichi, Kijev, Ukraine. Blue dots denote PSA samples analyzed in this study: 12.
610 Judkins, NE, USA; 13. Prairie Lake, NE, USA; 14. Obert, NE, USA; 15. Nussloch, Germany;
611 16. Mende, Hungary; 17. Dunaszekcső, Hungary; 18. Titel, Serbia; 19. Lingtai, China; 20.
612 Xifeng, China; 21. Beigoyuan, China; 22. Tumara Valley, NE–Siberia, Russia.
613 **Figure 2.** Kaolinite/chlorite (K/C) versus illite a), and smectite b) contents of PSA and
614 Greenland LGM dust samples. Data sources: B97–*Biscaye et al.* [1997]; S2000–*Svensson et*

615 *al.* [2000]; *Ú2012–Újvári et al.* [2012]. Error bars are not presented, but the overall
616 uncertainty is ~±10%.
617 **Figure 3.** Sr–Nd isotopic compositions of last glacial ice core dust and PSA samples in a)
618 with boxed area around Greenland dust, and likely potential sources enlarged in b); Nd–Hf
619 isotopic compositions of PSA samples analyzed in this study and comparison with those of
620 bulk loess and clay separates from the literature in c); d) PSA sample illite content versus
621 $\varepsilon_{Hf}(0)$ diagram. Note that error bars are not shown for the sake of figure clarity, but they are
622 mostly smaller than symbols of PSAs. Crosses denote isotopic data measured by TIMS at the
623 UV, Vienna, while bold crosses mark those obtained by TIMS/MC-ICP-MS at RHUL,
624 London and/or Leeds. All displayed data are from acetic acid treated loess size separates (<2
625 μm/<10 μm). Data sources for loess in Fig. 3a,b: B97–*Biscaye et al.* [1997]; S2000–*Svensson*
626 *et al.* [2000]; F09–*Feng et al.* [2009]; Ú2012–*Újvári et al.* [2012]; Z2015–*Zhao et al.* [2015].
627 Isotopic data of desert sand regions A, B, and C are from *Chen et al.* [2007]. LGM sediments
628 (W of Africa) and Saharan dust data originate from *Grousset et al.* [1988, 1992, 1998].
629 Circum-Pacific volcanic rocks isotopic data are from *Kepezhinskas et al.* [1997] and *George*
630 *et al.* [2003]. Black and gray hyperbola are mixing lines between end members EM_1, EM_2 and
631 EM_3. For end member compositions and mixing calculations see Text S1 (Supporting
632 Information). Data sources for Fig. 3c: bulk loess – *Chauvel et al.* [2014]; clay fractions of
633 loess in China – *Zhao et al.* [2015]. The Terrestrial, the Zircon-free/Zircon-bearing sediment,
634 and the Clay-sized arrays are from *Vervoort et al.* [2011], *Bayon et al.* [2009], and *Zhao et al.*
635 [2014].


1
2
3
4
22
10
9
8
19
7
21
20
5
6
13
12
14
GISP2
GRIP
11
15
16
17
18

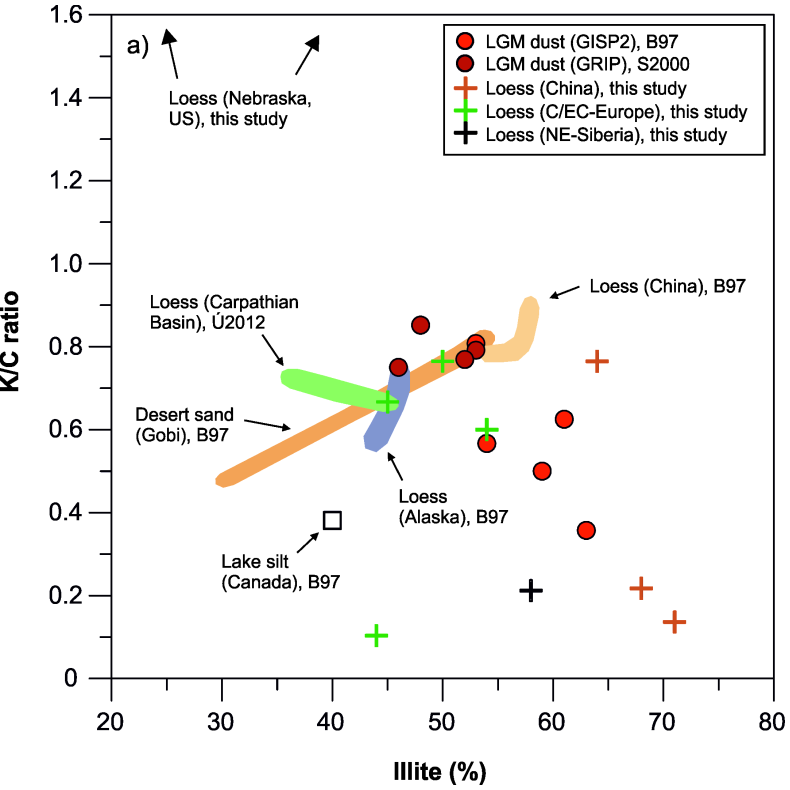
a)
LGM dust (GISP2), B97
LGM dust (GRIP), S2000
Loess (China), this study
Loess (C/EC-Europe), this study
Loess (NE-Siberia), this study
Loess (Nebraska, US), this study
Loess (China), B97
Loess (Carpathian Basin), Ú2012
Desert sand (Gobi), B97
Loess (Alaska), B97
Lake silt (Canada), B97
K/C ratio
Illite (%)
1.6
1.4
1.2
1.0
0.8
0.6
0.4
0.2
0
20
30
40
50
60
70
80

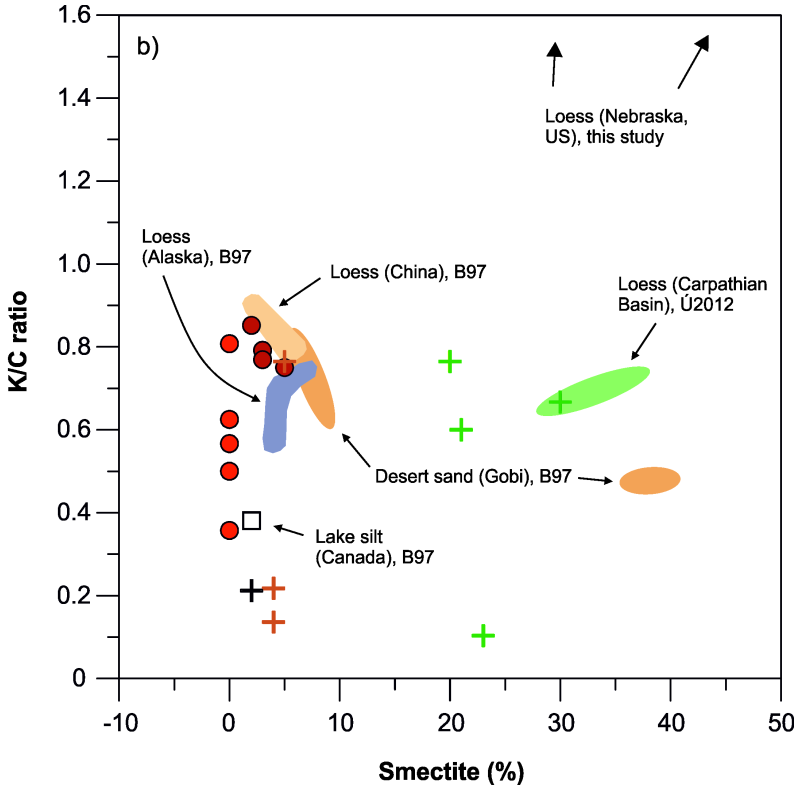
b)
Loess (Nebraska, US), this study
Loess (Alaska), B97
Loess (China), B97
Loess (Carpathian Basin), Ú2012
Desert sand (Gobi), B97
Lake silt (Canada), B97
K/C ratio
Smectite (%)
1.6
1.4
1.2
1.0
0.8
0.6
0.4
0.2
0
-10
0
10
20
30
40
50

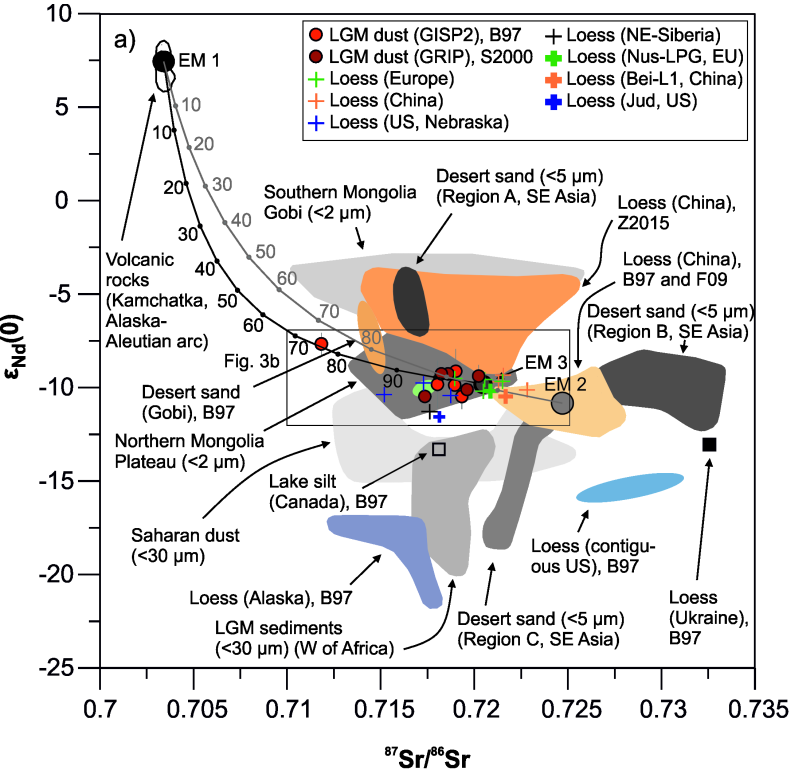
a)
LGM dust (GISP2), B97
LGM dust (GRIP), S2000
Loess (Europe)
Loess (China)
Loess (US, Nebraska)
Loess (NE-Siberia)
Loess (Nus-LPG, EU)
Loess (Bei-L1, China)
Loess (Jud, US)
EM 1
EM 2
EM 3
Volcanic rocks (Kamchatka, Alaska-Aleutian arc)
Southern Mongolia Gobi (<2 μm)
Desert sand (<5 μm) (Region A, SE Asia)
Loess (China), Z2015
Loess (China), B97 and F09
Desert sand (<5 μm) (Region B, SE Asia)
Fig. 3b
Desert sand (Gobi), B97
Northern Mongolia Plateau (<2 μm)
Lake silt (Canada), B97
Saharan dust (<30 μm)
Loess (contiguous US), B97
Loess (Alaska), B97
LGM sediments (<30 μm) (W of Africa)
Desert sand (<5 μm) (Region C, SE Asia)
Loess (Ukraine), B97
εNd(0)
87Sr/86Sr

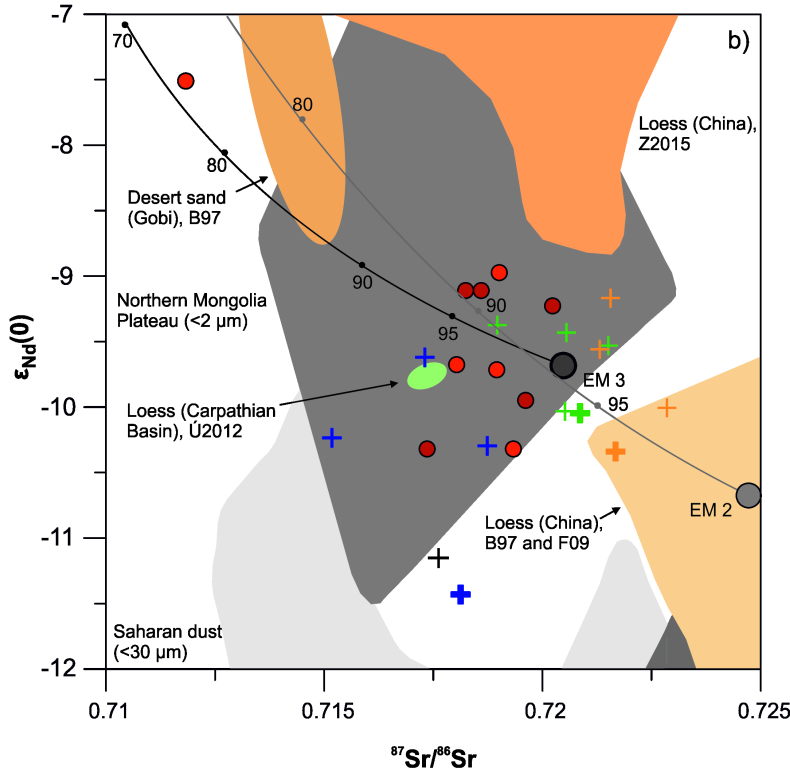
b)
Loess (China), Z2015
Desert sand (Gobi), B97
Northern Mongolia Plateau (<2 μm)
Loess (Carpathian Basin), Ú2012
Loess (China), B97 and F09
Saharan dust (<30 μm)
EM 2
EM 3
εNd(0)
87Sr/86Sr

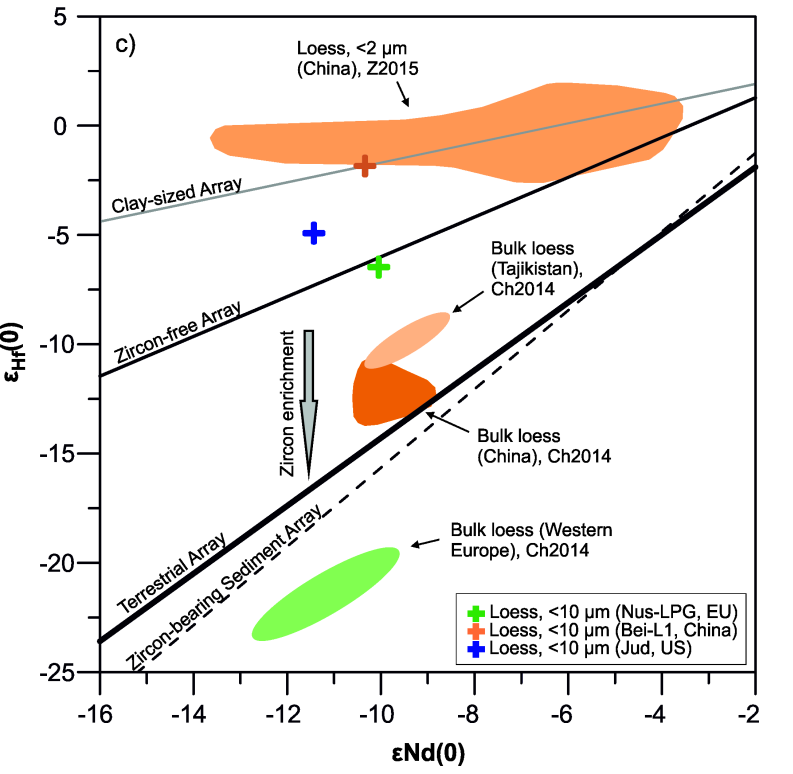
c)
Loess, <2 μm (China), Z2015
Clay-sized Array
Zircon-free Array
Bulk loess (Tajikistan), Ch2014
Zircon enrichment
Bulk loess (China), Ch2014
Terrestrial Array
Zircon-bearing Sediment Array
Bulk loess (Western Europe), Ch2014
Loess, <10 μm (Nus-LPG, EU)
Loess, <10 μm (Bei-L1, China)
Loess, <10 μm (Jud, US)
εHf(0)
εNd(0)

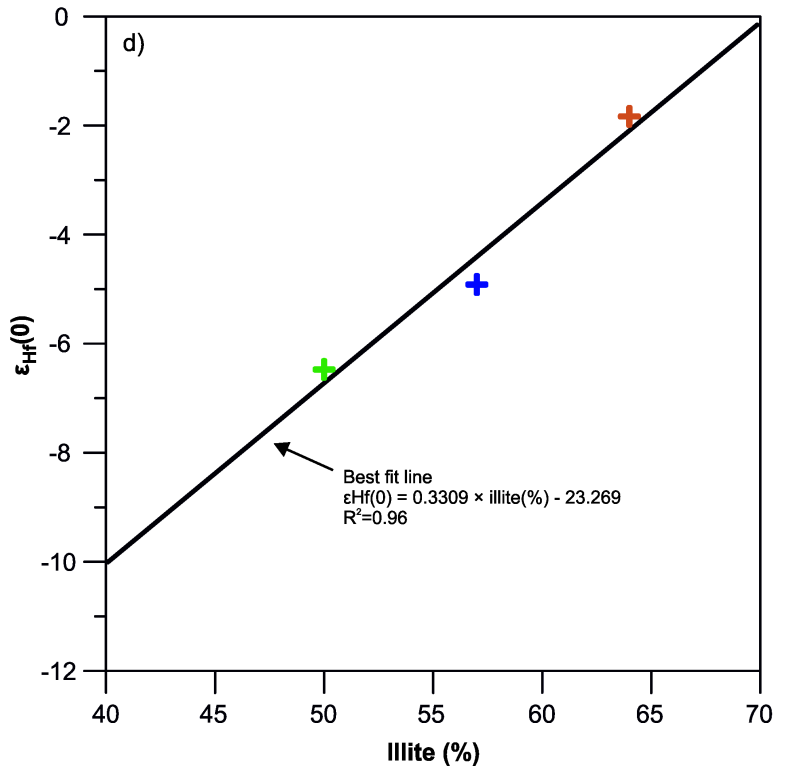
d)
Best fit line
εHf(0) = 0.3309 × illite(%) - 23.269
R²=0.96
εHf(0)
Illite (%)

Geophysical Research Letters

Supporting Information for

Two possible source regions for Central Greenland last glacial dust

Gábor Újvári[1,2], Thomas Stevens[3], Anders Svensson[4], Urs S. Klötzli[5], Christina Manning[6], Tibor Németh[1], János Kovács[7,8], Mark R. Sweeney[9], Martina Gocke[10], Guido L.B. Wiesenberg[10], Slobodan B. Markovic[11], Michael Zech[12]

[1]Institute for Geological and Geochemical Research, Research Centre for Astronomy and Earth Sciences, Hungarian Academy of Sciences, H-1112 Budapest, Budaörsi u. 45., Hungary
[2]Geodetic and Geophysical Institute, Research Centre for Astronomy and Earth Sciences, Hungarian Academy of Sciences, H-9400 Sopron, Csatkai E. u. 6-8., Hungary
[3]Department of Earth Sciences, Uppsala University, Villavägen 16, 75236 Uppsala, Sweden
[4]Centre for Ice and Climate, Niels Bohr Institute, University of Copenhagen, Juliane Maries Vej 30, 2100 Copenhagen, Denmark
[5]Department of Lithospheric Research, University of Vienna, Althanstraße 14, 1090 Vienna, Austria
[6]Department of Earth Sciences, Royal Holloway University of London, Egham, London, TW20 0EX, UK
[7]Department of Geology and Meteorology, University of Pécs, H-7624 Pécs, Ifjúság u. 6., Hungary
[8]Environmental Analytical and Geoanalytical Research Group, Szentágothai Research Centre, H-7624 Pécs, Ifjúság u. 20., Hungary
[9]Department of Earth Sciences, University of South Dakota, 414 E. Clark Street, Vermillion, SD 57069, USA
[10]Department of Geography, University of Zürich, Winterthurerstrasse 190, CH-8057 Zürich, Switzerland
[11]Laboratory for Palaeoenvironmental Reconstruction, Faculty of Sciences, University of Novi Sad, Trg Dositeja Obradovića 2, 21000 Novi Sad, Serbia
[12]Department of Soil Physics and Chair of Geomorphology, University of Bayreuth, Universitätsstrasse 30, D-95440 Bayreuth, Germany

Contents of this file

Introduction

This Supporting Information file contains a detailed description of samples, sampling strategies, and the applied procedures of XRD measurements as well as Sr-Nd-Hf isotopic analyses performed at the University of Vienna, Royal Holloway University of London, and the University of Leeds (Text S1). End-member compositions (shown in Fig. 3a,b) and mixing calculations are also specified in Text S1. Figure S1 displays the particle size distributions of size separates of five randomly selected loess samples, as determined by laser diffraction. Table S1 provides details on loess sampling sites, sample depths and approximate ages. Table S2 give information on the clay mineralogical compositions of potential source area samples (PSAs) investigated in this study, as determined from the XRD spectra. Finally, Sr-Nd-Hf isotopic compositions of PSAs, as measured by TIMS and MC-ICP-MS in the three different labs mentioned above, are given in Table S3.

Text S1.

Loess deposits are accumulations of both coarse and fine dust blown out from alluvial fans/floodplains of large river systems [*Smalley et al.,* 2009; *Stevens et al.,* 2013; *Újvári et al.,* 2013; *Nie et al.,* 2015] or deserts [*Sun,* 2002; *Yang and Ding,* 2008; *Lu et al.,* 2011], and provide an averaged composition of continental crust [*Taylor et al.,* 1983]. Loess deposits are made up of minerals originating from major dust emitting regions of glacial age and are also considered as potential Greenland dust source area samples in this study. Loess samples were collected at several locations around the Northern Hemisphere from North America to Asia (Table S1). The sampling strategy focused on collecting loess deposited at about the time of the LGM (~19-26 ka) [*Clark et al.,* 2009], the stratigraphic position of which we determined at each site using previously published radiocarbon and recent luminescence dating datasets (Table S1). All samples were taken from cleaned profiles.

Before mineralogical analyses, clay fractions (<2 μm) of loess samples were separated by sedimentation after removal of carbonates by leaching in 10% acetic acid. XRD measurements were then undertaken using a Philips PW 1710 diffractometer with CuKα radiation at 45 kV and 35 mA. Clay minerals were identified using XRD diagrams obtained from parallel-oriented specimens mounted on glass slides. All the calculations of clay mineral compositions from the XRD spectra strictly followed the semi-quantitative approach of *Svensson et al.* [2000], enabling a direct comparison of the PSAs' clay mineralogical compositions with those of ice core dust. Errors on reported clay mineral compositions are ~±10%.

Prior to Sr-Nd-Hf isotopic analyses, all samples were size-separated in distilled water (without adding chemical dispersant) according to Stokes Law to approximate the grain size of fine dust in ice cores, thereby excluding grain size effects on Sr isotopic ratios [*Dasch,* 1969; *Grousset and Biscaye,* 2005; *Feng et al.,* 2009; *Meyer et al.,* 2011; *Újvári et al.,* 2012]. Grain size distributions of some of these fine separates were checked using a Malvern Mastersizer 3000 laser particle analyzer and the distributions have modes at ~3-4 μm (Fig. S1), with some particles up to ~10 μm. For this reason we denote the fine separates as <10 μm fractions throughout in the

paper. After size separations carbonates were removed by leaching in weak acetic acid (0.5 mol/L) at room temperature for 8 h [*Biscaye et al.,* 1997; *Chen et al.,* 2007; *Újvári et al.,* 2012]. Secondary carbonates that are abundant in loess have lower $^{87}Sr/^{86}Sr$ isotopic ratios [*Capo et al.,* 1998] and can mask the signature of the aluminosilicate fraction which was analyzed in ice core dust samples [*Svensson et al.,* 2000]. To test the effects of acetic acid leaching on $^{87}Sr/^{86}Sr$, $^{143}Nd/^{144}Nd$ and $^{176}Hf/^{177}Hf$ isotope ratios, three samples (Bei-L1, Nus-LPG and Jud) were subjected to isotopic analyses before and after acid leaching. These samples were analyzed for Sr, Nd and Hf isotope compositions in the Geochemistry Laboratory, Royal Holloway University of London (RHUL), and the University of Leeds. These measurements also served to cross-check the Sr-Nd isotopic ratios determined on acetic acid treated size separates of PSA samples in the Laboratory of Geochronology, Department of Lithospheric Research, University of Vienna (UV). The procedures of isotopic analyses in these three labs were the following:

For Sr-Nd isotopic analyses in Vienna, 20 mg of each PSA sample (<10 μm fractions) was digested in tightly screwed Savillex beakers using an ultrapure mixture of HF: HNO_3 (4:1) for 2 weeks at 100-120 °C on a hot plate. Acid evaporation treatment of the residue with concentrated HNO_3 and 6 N HCl resulted in clear solutions. Element extraction (Sr, REE) was performed using AG 50W-X8 (200-400 mesh, Bio-Rad) resin and 2.5 N and 4.0 N HCl as eluents. Nd was separated from the REEs using teflon-coated HdEHP and 0.24 N HCl as eluent. Total procedural blanks were <1 ng for Sr and 50 pg for Nd, and are considered negligible. The pure element fractions were evaporated using a Re double filament assembly and run in static mode on a Thermo-Finnigan Triton TI TIMS machine in the Laboratory of Geochronology, UV, Vienna. A mean $^{87}Sr/^{86}Sr$ ratio of 0.710284±0.000004 (n=3; error is 2σ of the mean) was determined for the NBS987 (ref. value: $^{87}Sr/^{86}Sr$=0.710248; *Faure,* [2001]) and a mean $^{143}Nd/^{144}Nd$ ratio of 0.511846±0.000004 (n=2) for the La Jolla (ref. value: $^{143}Nd/^{144}Nd$=0.511858; *Lugmair and Carlson,* [1978]) international standards during the analysis period. Within-run mass fractionation was corrected for $^{88}Sr/^{86}Sr$=8.3752, and $^{146}Nd/^{144}Nd$ =0.7219, respectively. Uncertainties of isotopic ratios of PSA samples represent 2σ errors of the mean.

For Sr-Nd-Hf isotopic analyses at RHUL, approximately 50 mg of sample was weighed into Savillex beakers and digested in sub boiled HF:HNO_3 (4:1) for 48 hours. Whilst there was some evidence of graphite within the dissolved sample there was no sign of residual zircon. Samples were dried down and converted to nitric through the addition of concentrated HNO_3. Sr was extracted using Sr spec resin, with the Sr collection passed back through the resin to ensure good separation from Rb. Elutions were collected, evaporated and converted to HCl. These HCl fractions were passed through cation columns to separate Hf and LREE. Hf fractions were passed through LN columns under HCl-HF mixture to ensure good separation of Fe, Ti and Zr. LREE fractions were passed through LN columns under HCl to separate Nd from other LREE. Hf isotopes were determined using a VG IsoProbe MC-ICP-MS using a static analysis. JMC 475 (91ppb) standard run alongside the samples gave a mean value of 0.282184±0.000004 (n=3) within error of the long-term mean of 0.282180±0.000016 (n=30). Sr and Nd isotopes were analyzed on an Isotopx Phoenix TIMS using the multidynamic procedures of *Thirlwall,* [1991a,b]. Sr was loaded onto single Re filaments using a TaCl emitter. SRM987 (100ng) analyzed alongside the samples gave a value of 0.710234±0.000007, within error of the long-term mean of 0.710232±0.000010 (n=108). Nd was run as a metal (Nd^+) loaded onto Re side filaments using 1μl H_3PO_4 and loaded as a Re-Re-Ta triple filament assembly. Aldrich (200ng) analyzed alongside samples gave 0.511403±0.000003, within error of the long-term mean of 0.511407±0.000002 (n=39). Several samples were also analyzed for Nd^+ on the Thermo-Finnigan Triton TI TIMS at the University of

Leeds. Samples were run on double Re filament assemblies and analyzed in static mode for 240 ratios. Samples analyzed for Nd^+ at both RHUL and Leeds show good agreement in $^{143}Nd/^{144}Nd$ values.
$^{143}Nd/^{144}Nd$ and $^{176}Hf/^{177}Hf$ ratios in this study are reported as: $\varepsilon_{Nd}(0)=((^{143}Nd/^{144}Nd_{sample}/^{143}Nd/^{144}Nd_{CHUR})-1)\times10^4$, and $\varepsilon_{Hf}(0)=((^{176}Hf/^{177}Hf_{sample}/^{176}Hf/^{177}Hf_{CHUR})-1)\times10^4$, using the present-day chondritic uniform reservoir (CHUR) values of 0.512630±0.000011 and 0.282785±0.000011, respectively [*Bouvier et al.*, 2008].

End member compositions displayed in Fig. 3a,b are the following. End-member$_1$=EM_1 (Sr: 413 ppm, Nd: 13.6 ppm, $^{87}Sr/^{86}Sr$: 0.703400, $^{143}Nd/^{144}Nd$: 0.513019) is the mean of Kamchatka-Aleutian arc volcanics. EM_2 (Sr: 112.1 ppm, Nd: 18.2 ppm, $^{87}Sr/^{86}Sr$: 0.724725, $^{143}Nd/^{144}Nd$: 0.512083) is the mean of Chinese loess based on data of loess size separates (<5 μm) published by *Biscaye et al.* [1997] and *Feng et al.* [2009], excluding the loess samples measured in this study. EM_3 (Sr: 124 ppm, Nd: 33 ppm, $^{87}Sr/^{86}Sr$: 0.720480, $^{143}Nd/^{144}Nd$: 0.512134) is the mean of European loess. Sr-Nd isotopic compositions of EM_3 are based on loess sample separates measured in this study. Sr and Nd concentrations of EM_3 are unpublished ICP-MS data of G. Újvári from acetic acid treated size separates (<5 μm) of Hungarian loess samples (Paks, Mende sites). For more information see *Újvári et al.* [2012]. Mixing hyperbolae are calculated from the above defined Sr, Nd concentrations and isotopic data using the equations given in *Faure* [2001].

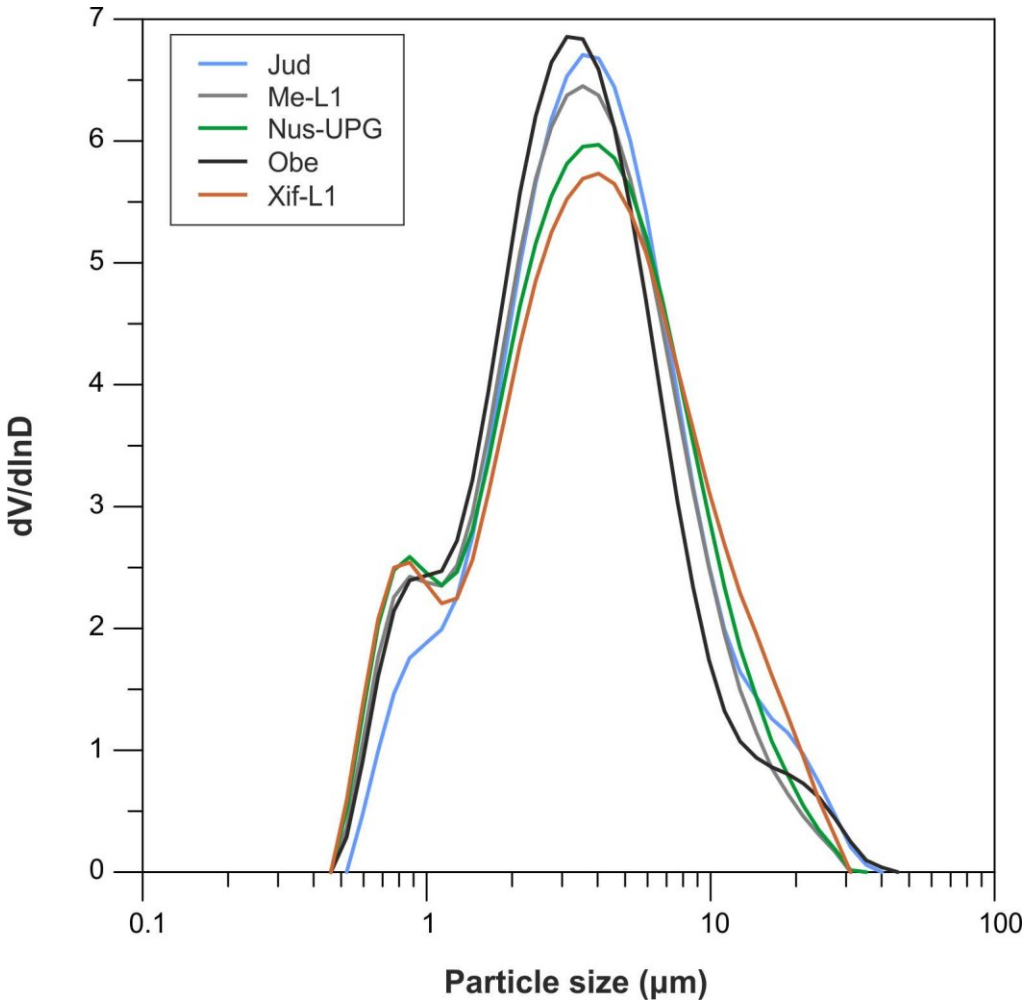

Figure S1. Particle size distributions of five randomly chosen loess grain size separates. For sample codes see Table S1.

Site location	Region	Latitude	Longitude	Sample code	Depth in profile (m)	Age (ka)
Beigoyuan, China	SE Asia	36°37'36"N	107°16'57"E	Bei-L1	4.5	20
Lingtai, China	SE Asia	35°00'33"N	107°30'33"E	Lin-L1	6	20-50
Xifeng, China	SE Asia	34°45'N	107°49'E	Xif-L1	3.4-3.6	25
Nussloch, Germany	Central Europe	49°18'59"N	8°43'54"E	Nus-UPG	3.4-3.5	20-25
Dunaszekcső, Hungary	East Central Europe	46°05'25"N	18°45'44"E	Dsz-Pr1	5	23-25
Mende, Hungary	East Central Europe	45°25'32"N	19°26'51"E	Me-L1	4.7	10-24
Titel, Serbia	East Central Europe	45°14'N	20°19'E	Tit-L1	3	20-30
Tumara valley, NE Siberia, Russia	NE Asia	63°36'N	129°58'E	Sib200	2	10-30
Judkins, Nebraska, USA	North America	41°29'N	100°11'W	Jud	not specified	12-28
Obert, Nebraska, USA	North America	42°41'N	97°01'W	Obe	not specified	12-28
Prairie Lake, Nebraska, USA	North America	40°32'N	98°30'W	Pra	not specified	12-28

Source of site and sample information, including absolute ages: Beigoyuan - *Stevens et al.,* [2008]; Lingtai - *Zhu et al.,* [2000]; Xifeng - *Jahn et al.,* [2001]; Nussloch - *Lang et al.,* [2003], *Gocke et al.,* [2014]; Dunaszekcső - *Újvári et al.,* [2014]; Mende - *Frechen et al.,* [1997]; Tumara - *Zech et al.,* [2007]; Titel - *Bokhorst et al.,* [2011]; Judkins, Obert and Prairie Lake - *Sweeney and Mason,* [2013]

Table S1. Potential source area samples analyzed in the current study with information on location and sampling.

Sample code	Region	Quartz	Feldspars	Illite	Chlorite	Kaolinite	Smectite	K/C
Bei-L1	SE Asia	7	1	64	17	13	5	0.76
Lin-L1	SE Asia	9	1	71	22	3	4	0.14
Xif-L1	SE Asia	10	1	68	23	5	4	0.22
Nus-UPG	Central Europe	12	1	50	17	13	20	0.76
Dsz-Pr1	East Central Europe	12	1	54	15	9	21	0.60
Me-L1	East Central Europe	10	0	45	9	6	30	0.67
Tit-L1	East Central Europe	12	1	44	29	3	23	0.10
Sib200	NE Asia	20	3	58	33	7	2	0.21
Jud	North America	14	2	57	3	11	29	3.67
Obe	North America	10	1	14	1	9	75	9.00
Pra	North America	7	0	23	0	7	71	u.d.

*To calculate mineral compositions the method of *Svensson et al.* [2000] was followed
u.d.=undefined

Table S2. Semi-quantitative mineral composition (%) of the clay fraction (<2 μm) of potential source area samples based on the recorded XRD spectra*

Sample code	Fraction	Acid treatment[a]	Laboratory[b]	$^{87}Sr/^{86}Sr$	$2\sigma_m$[c]	$^{143}Nd/^{144}Nd$	$2\sigma_m$[c]	εNd(0)[d]	2σ[e]	$^{176}Hf/^{177}Hf$	$2\sigma_m$[c]	εHf(0)[f]	2σ[g]
Bei-L1	<10 µm	untreated	RHUL, London	0.712987	0.000007	0.512114	0.000005	-10.1	0.24	0.282704	0.000015	-2.9	0.66
Bei-L1	<10 µm	acetic acid	RHUL, London	0.721676	0.000006	0.512100	0.000004	-10.3	0.23	0.282733	0.000016	-1.8	0.69
Bei-L1	<10 µm	acetic acid	UV, Vienna	0.721314	0.000004	0.512140	0.000003	-9.6	0.22				
Lin-L1	<10 µm	acetic acid	UV, Vienna	0.721560	0.000004	0.512160	0.000002	-9.2	0.22				
Xif-L1	<10 µm	acetic acid	UV, Vienna	0.722854	0.000004	0.512117	0.000003	-10.0	0.22				
Nus-UPG	<10 µm	untreated	RHUL, London	0.710762	0.000008					0.282611	0.000015	-6.2	0.66
Nus-UPG	<10 µm	untreated	University of Leeds			0.512119	0.000008	-10.0	0.27				
Nus-UPG	<10 µm	acetic acid	RHUL, London	0.720862	0.000006	0.512115	0.000004	-10.0	0.23	0.282602	0.000012	-6.5	0.58
Nus-UPG	<10 µm	acetic acid	University of Leeds			0.512130	0.000033	-9.8	0.68				
Nus-UPG	<10 µm	acetic acid	UV, Vienna	0.718965	0.000004	0.512149	0.000003	-9.4	0.22				
Dsz-Pr1	<10 µm	acetic acid	UV, Vienna	0.720549	0.000004	0.512147	0.000003	-9.4	0.22				
Me-L1	<10 µm	acetic acid	UV, Vienna	0.720515	0.000004	0.512116	0.000003	-10.0	0.22				
Tit-L1	<10 µm	acetic acid	UV, Vienna	0.721510	0.000004	0.512141	0.000003	-9.5	0.22				
Sib200	<10 µm	acetic acid	UV, Vienna	0.717621	0.000003	0.512058	0.000004	-11.2	0.23				
Jud	<10 µm	untreated	RHUL, London	0.712824	0.000008	0.512079	0.000003	-10.7	0.22	0.282634	0.000012	-5.3	0.58
Jud	<10 µm	untreated	University of Leeds			0.512077	0.000006	-10.8	0.24				
Jud	<10 µm	acetic acid	RHUL, London	0.718125	0.000010	0.512044	0.000022	-11.4	0.48	0.282646	0.000013	-4.9	0.60
Jud	<10 µm	acetic acid	University of Leeds			0.512045	0.000015	-11.4	0.36				
Jud	<10 µm	acetic acid	UV, Vienna	0.718735	0.000004	0.512102	0.000003	-10.3	0.22				
Obe	<10 µm	acetic acid	UV, Vienna	0.717305	0.000012	0.512137	0.000003	-9.6	0.22				
Pra	<10 µm	acetic acid	UV, Vienna	0.715178	0.000004	0.512105	0.000003	-10.2	0.22				

[a]Acid treatment was performed using 0.5 mol/L acetic acid

[b]Sr-Nd-Hf isotopic compositions were measured by MC-ICP-MS and TIMS at the Royal Holloway University, London (RHUL) and the University of Leeds, while Sr-Nd isotopic compositions were analyzed by TIMS in the laboratory of the University of Vienna (UV)

[c]Standard error of the mean

[d]$\varepsilon Nd(0) = (^{143}Nd/^{144}Nd_{sample}/^{143}Nd/^{144}Nd_{CHUR} - 1)*10000$, where $^{143}Nd/^{144}Nd_{CHUR}=0.512630\pm0.000011$ [*Bouvier et al.,* 2008]

[e]Errors of εNd(0) were propagated as

$$\sqrt{\left(\frac{\partial \varepsilon}{\partial x}\sigma_x\right)^2 + \left(\frac{\partial \varepsilon}{\partial y}\sigma_y\right)^2} = \sqrt{\left(\frac{1}{y}10000\sigma_x\right)^2 + \left(-\frac{x}{y^2}10000\sigma_y\right)^2}$$

, where ε=εNd(0), $x=^{143}Nd/^{144}Nd_{sample}$, $y=^{143}Nd/^{144}Nd_{CHUR}$, σ_x=uncertainty of x and σ_y=uncertainty of y

[f]εHf(0) = ($^{176}Hf/^{177}Hf_{sample}/^{176}Hf/^{177}Hf_{CHUR}$ - 1)*10000, where $^{176}Hf/^{177}Hf_{CHUR}$=0.282785±0.000011 [*Bouvier et al.,* 2008]

[g]Errors of εHf(0) were propagated as those of εNd(0), but with ε=εHf(0), $x=^{176}Hf/^{177}Hf_{sample}$, $y=^{176}Hf/^{177}Hf_{CHUR}$, σ_x=uncertainty of x and σ_y=uncertainty of y

Table S3. Sr, Nd and Hf isotopic compositions of the fine (<10 µm) fractions of potential source area samples

References

Biscaye, P.E., F.E. Grousset, M. Revel, S. Van der Gaast, G.A. Zielinski, A. Vaars, and G. Kukla (1997), Asian provenance of glacial dust (stage 2) in the Greenland Ice Sheet Project 2 Ice Core, Summit, Greenland, *J. Geophys. Res.,* 102, 26765-26781.

Bokhorst, M.P., J. Vandenberghe, P. Sümegi, M. Lanczont, N.P. Gerasimenko, Z.N. Matviishina, S.B. Markovic, and M. Frechen (2011), Atmospheric circulation patterns in central and eastern Europe during the Weichselian Pleniglacial inferred from loess grain-size records, *Quatern. Int.,* 234, 62-74.

Bouvier, A., J.D. Vervoort, and P.J. Patchett (2008), The Lu–Hf and Sm–Nd isotopic composition of CHUR: Constraints from unequilibrated chondrites and implications for the bulk composition of terrestrial planets, *Earth Planet. Sc. Lett., 273*, 48-57.

Capo R.C., B.W. Stewart, and O.A. Chadwick (1998), Strontium isotopes as tracers of ecosystem processes: theory and methods, *Geoderma,* 82, 197-225.

Chen, J., G. Li, J. Yang, W. Rao, H. Lu, W. Balsam, Y. Sun, and J. Ji (2007), Nd and Sr isotopic characteristics of Chinese deserts: implications for the provenances of Asian dust, *Geochim. Cosmochim. Ac.,* 71, 3904-3914.

Clark, P.U., A.S. Dyke, J.D. Shakun, A.E. Carlson, J. Clark, B. Wohlfarth, J.X. Mitrovica, S.W. Hostetler, and A.M. McCabe (2009), The Last Glacial Maximum, *Science,* 325, 710-714.

Dasch, E.J. (1969), Strontium isotopes in weathering profiles, deep-sea sediments, and sedimentary rocks, *Geochim. Cosmochim. Ac.,* 33, 1521-1552.

Faure, G. (2001), Origin of igneous rocks: the isotopic evidence, Springer-Verlag, Berlin, Heidelberg.

Feng, J.-L., L.-P. Zhu, X.-L. Zhen, Z.-G. Hu (2009), Grain size effect on Sr and Nd isotopic compositions in eolian dust: Implications for tracing dust provenance and Nd model age, *Geochem. J.,* 43, 123-131.

Frechen, M.A., E. Horváth, and Gy. Gábris (1997), Geochronology of middle and upper Pleistocene loess sections in Hungary, *Quaternary Res.,* 48, 291-312.

Gocke, M., U. Hambach, E. Eckmeier, L. Schwark, L. Zöller, M. Fuchs, M. Löscher, G.I.B. Wiesenberg (2014), Introducing an improved multi-proxy approach for paleoenvironmental reconstruction of loess–paleosol archives applied on the Late Pleistocene Nussloch sequence (SW Germany). *Palaeogeogr., Palaeocl.,* 410, 300–315.

Grousset, F.E., and P.E. Biscaye (2005), Tracing dust sources and transport patterns using Sr, Nd and Pb isotopes, *Chem. Geol.,* 222, 149-167.

Jahn, B., S. Gallet, and J. Han (2001), Geochemistry of the Xining, Xifeng and Jixian sections, Loess Plateau of China: eolian dust provenance and paleosol evolution during the last 140 ka, *Chem. Geol.,* 178, 71-94.

Lang, A., C. Hatté, D.-D. Rousseau, P. Antoine, M. Fontugne, L. Zöller, and U. Hambach (2003), High-resolution chronologies for loess: comparing AMS 14C and optical dating results, *Quaternary Sci. Rev.,* 22, 953-959.

Lu, H., Mason, J.A., Stevens, T., Zhou, Y., Yi, S., and X. Miao (2011), Response of surface processes to climatic change in the dunefields and Loess Plateau of North China during the late Quaternary, *Earth Surf. Proc. Land.,* 36, 1590-1603.
Lugmair, G.W., and R.W., Carlson (1978), The Sm–Nd history of KREEP, in: Proc. 9th Lunar Planet. Sci. Conf.. pp. 689-704.
Meyer, I., G.R. Davies, and J.-B.W. Stuut (2011), Grain size control on Sr–Nd isotope provenance studies and impact on paleoclimate reconstructions: an example from deep sea sediments offshore NW Africa, *Geochem. Geophy. Geosy.,* 12, Q03005. doi:10.1029/2010GC003355.
Nie, J., T. Stevens, M. Rittner, D. Stockli, E. Garzanti, M. Limonta, A. Bird, S. Ando, P. Vermeesch, J. Saylor, H. Lu, D. Breecker, X. Hu, S. Liu, A. Resentini, G. Vezzoli, W. Peng, A. Carter, S. Ji, and B. Pan (2015), Loess Plateau storage of Northeastern Tibetan Plateau-derived Yellow River sediment, *Nat. Commun.*, 6, 8511, doi: 10.1038/ncomms9511.
Smalley, I., K. O'Hara-Dhand, J. Wint, B. Machalett, Z. Jary, and I. Jefferson (2009), Rivers and loess: the significance of long river transportation in the complex event sequence approach to loess deposit formation, *Quatern. Int.,* 198, 7-18.
Stevens, T., A. Carter, T.P. Watson, P. Vermeesch, S. Andó, A.F. Bird, H. Lu, E. Garzanti, M.A. Cottam, I. Sevastjanova (2013), Genetic linkage between the Yellow River, the Mu Us desert and the Chinese Loess Plateau, *Quaternary Sci. Rev.,* 78, 355-368.
Stevens, T., H. Lu, D.S.G. Thomas, and S.J. Armitage (2008), Optical dating of abrupt shifts in the Late Pleistocene East Asian monsoon, *Geology*, 36, 415-418.
Sun, J.M. (2002), Provenance of loess material and formation of loess deposits on the Chinese Loess Plateau, *Earth Planet. Sc. Lett.,* 203, 845-859.
Svensson, A., P.E. Biscaye, and F.E. Grousset (2000), Characterization of late glacial continental dust in the Greenland Ice Core Project ice core, *J. Geophys. Res.,* 105, 4637-4656.
Sweeney, M.R., and J.A. Mason (2013), Mechanisms of dust emission from Pleistocene loess deposits, Nebraska, USA, *J. Geophys. Res.,* 118, 1460-1471.
Taylor, S.R., S.M. McLennan, and M.T. McCulloch (1983), Geochemistry of loess, continental crustal composition and crustal model ages, *Geochim. Cosmochim. Ac.,* 47, 1897-1905.
Thirlwall, M.F. (1991a), High-precision multicollector isotopic analysis of low levels of Nd as oxide, *Chem. Geol.,* 94, 13-22.
Thirlwall, M.F. (1991b), Long-term reproducibility of multicollector Sr and Nd isotope ratio analysis, *Chem. Geol.,* 94, 85-104.
Újvári, G., U. Klötzli, F. Kiraly, and T. Ntaflos (2013), Towards identifying the origin of metamorphic components in Austrian loess: insights from detrital rutile chemistry, thermometry and U–Pb geochronology, *Quaternary Sci. Rev.,* 75, 132-142.
Újvári, G., M. Molnár, Á. Novothny, B. Páll-Gergely, J. Kovács, and A. Várhegyi (2014), AMS 14C and OSL/IRSL dating of the Dunaszekcső loess sequence (Hungary): chronology for 20 to 150 ka and implications for establishing reliable age-depth models for the last 40 ka, *Quaternary Sci. Rev.,* 106, 140-154.
Újvári, G., A. Varga, F.C. Ramos, J. Kovács, T. Németh, and T. Stevens (2012), Evaluating the use of clay mineralogy, Sr-Nd isotopes and zircon U-Pb ages in tracking dust provenance: An example from loess of the Carpathian Basin, *Chem. Geol.,* 304–305, 83-96.
Yang, S., and Z. Ding (2008), Advance-retreat history of the East-Asian summer monsoon rainfall belt over northern China during the last two glacial-interglacial cycles, *Earth Planet. Sc. Lett.,* 274, 499-510.
Zech, M., R. Zech, and B. Glaser (2007), A 240,000-year stable carbon and nitrogen isotope record from a loess-like palaeosol sequence in the Tumara Valley, Northeast Siberia, *Chem. Geol.,* 242, 307-318.
Zhu, R., B. Guo, Y. Pan, Q. Liu, A. Zeman, and V. Suchy (2000), Reliability of geomagnetic secular variations recorded in a loess section at Lingtai, north-central China, *Sci. China Ser. D,* 43, 1-9.